Sensors and Materials, Vol. 37, No. 5 (2025) 1835–1851
MYU Tokyo

S & M 4021

Development of a Chitosan Nanosilver Composite as Surface-enhanced Raman-scattering-based Sensor for Bisphenol A Detection

Yan-Ting Chen,[1] Shih-Chen Shi,[1*] and Dieter Rahmadiawan[1,2]

[1]Department of Mechanical Engineering, National Cheng Kung University (NCKU), No.1, University Road, Tainan 70101, Taiwan
[2]Department of Mechanical Engineering, Universitas Negeri Padang, 25173 Padang, Sumatera Barat, Indonesia

(Received November 5, 2024; accepted April 21, 2025)

Keywords: chitosan, SERS-based detection, nanosilver, plasticizer, BPA sensor

Plastics are extensively used worldwide, with bisphenol A (BPA), produced in quantities exceeding 6 billion pounds annually, standing out as a commonly utilized plasticizer. BPA is known to leach into foods and beverages from containers and can also migrate from dental sealants and composite materials during everyday use. The widespread presence of BPA in daily life highlights an urgent need for rapid and sensitive detection methods to monitor and mitigate potential health risks from BPA exposure. In this study, we introduce a sustainable and eco-friendly approach to developing a simple, one-step surface-enhanced Raman-scattering (SERS)-based sensor substrate for BPA detection. This approach creates in situ reduction sites in a colloidal solution by leveraging chitosan's properties as a cationic polymer, enabling precise control over silver ion reduction and optimizing particle size and distribution. Additionally, polyols rich in hydroxyl groups are incorporated to counteract chain scission in chitosan during the reduction process, whereby molecular chains are extended and the sensor is stabilized. This innovative process converts the colloidal solution into a film, yielding a highly efficient, one-step SERS-based sensor substrate for detecting BPA in various environments.

1. Introduction

The Industrial Revolution of the 1760s marked significant progress for humanity but also introduced environmental challenges. Factories near rivers often released untreated wastewater, contributing to pollution.(1) Post-World War II, the rise of plastics, facilitated by the booming chemical industry, further exacerbated environmental pollution. During this era, "environmental hormones", chemicals that mimic human hormones and disrupt the endocrine system, were introduced.(2) Many chemicals, including dichlorodiphenyltrichloroethane (DDT), di(2-ethylhexyl)phthalate (DEHP), and bisphenol A (BPA), are classified as such, and pose risks like cancer and developmental abnormalities.(3,4) Moreover, BPA, which can be found in almost everything from food containers to dental sealants, has been linked to cardiovascular complications.(5)

*Corresponding author: e-mail: scshi@mail.ncku.edu.tw
https://doi.org/10.18494/SAM5447

ISSN 0914-4935

Surface-enhanced Raman scattering (SERS) has emerged as a powerful analytical tool capable of detecting low-concentration pollutants and biological molecules owing to its capability to amplify Raman scattering signals.[6] Commercial SERS substrates, however, face significant limitations that hinder their practical applications. These substrates rely heavily on noble metals like gold and silver for their plasmonic properties, which makes them costly and unsustainable for large-scale use.[7–9] Additionally, most conventional SERS substrates are non-biodegradable, raising concerns about their environmental impact when disposed of.[10]

In recent decades, the interest in natural materials among researchers has surged, driven by not only environmental concerns but also by the discovery of their unique properties, which are comparable to those of conventional materials.[11–15] One such material is chitin. As the world's second-most abundant natural polymer, chitin and its derivative, chitosan, present promising solutions. Chitosan, known for its biodegradability and biocompatibility, has applications ranging from drug delivery to the synthesis of metal nanoparticles.[16–18] It is crucial in producing biocompatible SERS substrates. These substrates can detect low-concentration substances, including environmental pollutants, by amplifying Raman scattering signals.[19] The dispersion, mechanical reinforcement, and control of optical properties in nanomaterial systems are critical for developing efficient sensing materials;[20–22] these principles guide the design of our chitosan nanosilver composite for sensitive and stable BPA detection.

This study is focused on environmental sustainability, aiming to use natural, reusable, and eco-friendly materials to facilitate waste recycling and reuse and thus achieve the so-called green cycle.[23] The exploration is focused on whether naturally abundant materials can simultaneously address heavy-metal pollution and endocrine disruptor issues, by detecting substances like BPA, which mimics estrogen by binding to its receptors, disrupting hormonal signaling and causing developmental and metabolic abnormalities. SERS is a current emerging research direction, and in this study, we propose to leverage the chelating properties of chitosan with metal ions to achieve control over metal particle size and dispersion through careful selection of the processing parameters. Chelating refers to the capability of chitosan's functional groups, such as amino and hydroxyl groups, to form stable coordination bonds with metal ions. This interaction helps anchor metal ions onto the polymer matrix, facilitating the controlled reduction and uniform dispersion of nanoparticles. The goal is to achieve environmental sustainability by utilizing chitosan composites with moderate and uniformly dispersed metal particle sizes as metal-enhanced SERS substrates for detecting pollutants such as ecological hormones. This approach transforms the initial metal pollutants into valuable resources that amplify the detection signals of additional contaminants. This process realizes the aim of a sustainable cycle, leveraging the biodegradability of chitosan.

In this study, we emphasize chitosan's role in nanoparticle synthesis, particularly for environmental sustainability applications. By leveraging chitosan's properties, we aim to create SERS substrates that can efficiently detect pollutants like BPA. Our goal is to transform metal pollutants into resources for detecting additional contaminants, thereby promoting a sustainable cycle of waste recycling and reuse. This approach not only addresses heavy-metal pollution but also offers a green solution to the problem of environmental hormones, leveraging the biodegradability of chitosan for environmental restoration efforts. The intersection of

environmental sustainability and nanotechnology, particularly through the use of chitosan in creating SERS substrates, represents a promising direction for addressing the dual challenges of pollution and endocrine disruptors. This study demonstrates the potential of natural, reusable materials in crafting solutions that benefit both human health and the environment.

2. Materials and Experiment

2.1 Materials

Chitosan was purchased from Charming & Beauty Co., Ltd. (Taipei, Taiwan). Silver nitrate ($AgNO_3$), used as the silver precursor, was sourced from Sigma-Aldrich and had a purity of 99.9%. Acetic acid, used as a reducing agent, was obtained from PanReac Applichem (Barcelona, Spain). Polyols such as L-arabinose and xylitol, used as plasticizers to prevent chitosan chain scission during the reduction process, were obtained from Uni-Onward Corp. (New Taipei, Taiwan). Crystal violet dye was used in SERS testing to determine the detection capabilities of the substrate. All reagents were used as received without further purification.

2.2 Green reduction of nanoparticles

Chitosan was dissolved into an aqueous acetic acid solution to prepare a colloidal solution with attached sites. Silver nitrate powder was then dissolved in ultrapure water, and the colloidal solution was mixed with silver nitrate. The mixture was placed on an electromagnetic stirrer and heated until it reached 100 °C. Subsequently, acetic acid was added to the mixture, which was then stirred continuously at 450 rpm while maintaining the temperature at 100 °C for four hours. The experiment's sample codes are presented in Table 1.

2.3 One-step SERS substrate-film formation and characterization

The reduced chitosan composite silver nanoparticle solution is limited to 20 wt% polyol plasticizer addition, which is the optimal amount determined by experimentation. The plasticizer was uniformly mixed using an electromagnetic heating stirrer and an oscillator, and finally, the mixture was poured into a petri dish and dried in a 60 °C oven for 48 h. The substance to be tested was placed on the one-step SERS substrate obtained after drying and then analyzed using a micro-Raman spectrometer.

Table 1
Sample codes for the experiment.

Experiment parameters	Code
X wt% Chitosan + Y wt% acetic acid	CXAY
X wt% Chitosan + Y wt% Silver nitrate	CXSY
Chitosan + X wt% L-Arabinose	C@LX
Chitosan + X wt% L-Arabinose + Y wt% Xylitol	C@LXXY

2.4 Nanoparticle analysis

The formation of bonds between chitosan and nanoparticles during the reduction process was determined by Fourier-transform infrared spectroscopy (FTIR). The silver nanoparticle size and structure were observed by high-resolution field emission scanning/transmission electron microscopy (FESTEM).

2.5 SERS performance

Crystal violet is frequently chosen as an analyte for SERS performance analysis owing to its affordability, water solubility, sensitivity, and efficient signal production, making it highly suitable for evaluating its effectiveness. Several concentrations were prepared using a 10-fold dilution method to test the substrate's minimum detection concentration. The intensity of the analyte was measured, and along with the concentration of the analyte dropped onto the glass substrate, the SERS enhancement factor (EF) of this experimental substrate can be calculated.

3. Results and Discussion

3.1 Detection of reduced silver nanoparticles

Fourier-transform infrared spectroscopy (FTIR) was employed to compare pure chitosan with chitosan used to reduce silver nanoparticles. As depicted in Fig. 1, the findings revealed notable changes after the reduction reaction. Specifically, a shift at 1030 cm^{-1} in the C–O stretch suggests that oxygen atoms in hydroxyl groups may bond hydrogen with metal particles.[24,25] Other shifts observed at 1660 and 1598 cm^{-1}, corresponding to the $CONH_2$ and NH_2 groups, respectively, indicate that chitosan transforms into NH3+ cationic polymers during reduction.[26]

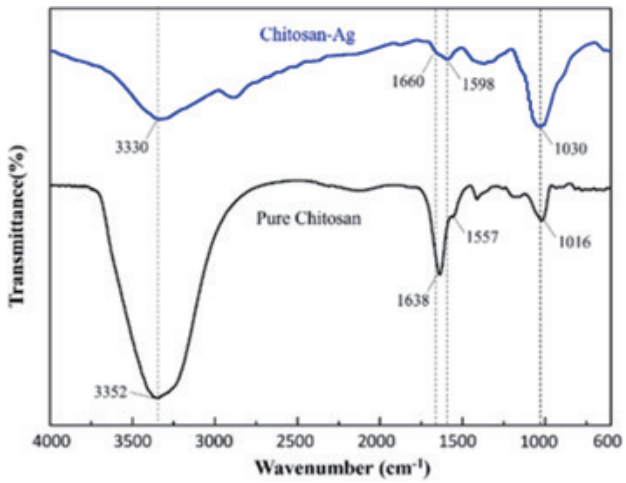

Fig. 1. (Color online) FTIR observations of bonding between chitosan and chitosan–Ag nanoparticles.

Moreover, a notable decrease in the intensity of the band between 3300 and 3500 cm^{-1}, associated with amino stretching vibrations, indicates a decrease in the number of amino groups.[27] This reduction is probably a consequence of the amino groups donating electrons to the metal to form bonds.

The morphology of the chitosan–Ag and pure silver nanoparticles is depicted in Figs. 2(a) and 2(b), respectively. Table 2 shows the lattice spacing (d-spacing in Ångströms) along with standard reference values obtained from the Ag Powder Diffraction File (PDF) card No. 00-004-0788, which provides crystallographic data for pure silver. Both nanoparticles exhibit a spheroidal morphology with visible facets, indicative of crystalline planes.[27] The variation in shape and size suggests a polydisperse distribution. It can be seen from Figs. 2(a) and 2(b) that the chitosan–Ag nanoparticles are smaller in size than the pure silver nanoparticles. This confirms that the use of chitosan in the synthesis of silver nanoparticles can lead to a reduction in particle size.

Furthermore, the presence of multiple diffraction rings in the TEM images indicates that the nanoparticles are polycrystalline.[28] From the d-spacing values listed in Table 2, we can conclude that the nanoparticles are well crystallized, and the observed rings correspond to the planes expected for a face-centered cubic (fcc) lattice.

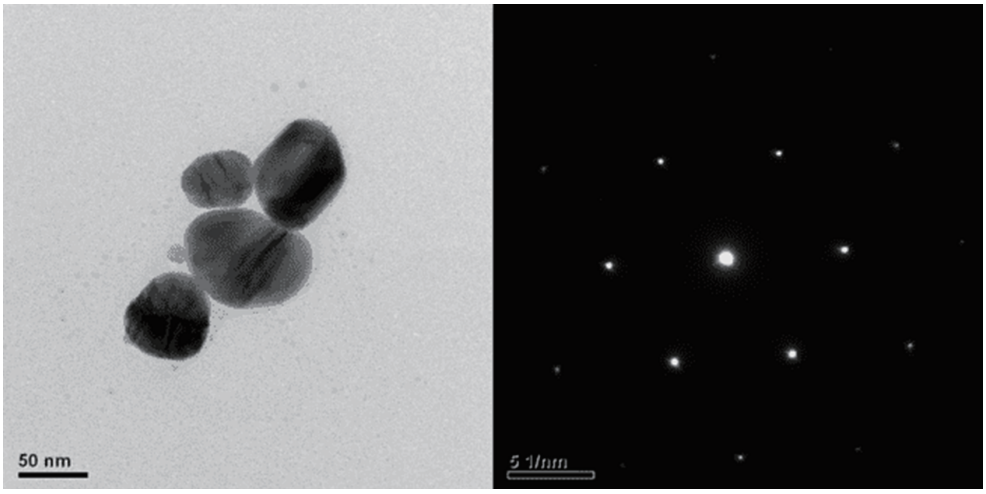

(a) (b)

Fig. 2. (a) TEM images and (b) electron diffraction patterns of Ag nanoparticles.

Table 2
d-Spacing and standard spectra to verify lattice structure.

	Ag PDF 00-004-0788, d-spacing (Å)	Calculated D (Å)	(h k l)
Ag	2.0440	2.0426	2 0 0
	1.4450	1.4564	2 2 0
	0.9375	0.9372	3 3 1
	1.0215	1.0398	4 0 0
	0.8341	0.8418	4 2 2

3.2 Size control of metal particles

Employing chitosan alone for particle reduction proves to be time-consuming. To address this issue, we introduce ascorbic acid as a catalyst, which supplies free electrons for the redox reaction with metal ions, to significantly reduce the reaction time. The challenge, however, resides in controlling the size of the nanoparticles produced by this method. To mitigate this problem, manipulating variables such as the pH value and chitosan concentration is suggested to reduce and control the size of the nanoparticles more effectively. Although chitosan is not hydrophilic, it can dissolve in acidic solutions to form cationic polymers, which are crucial in the nanoparticle reduction process.

The complete dissolution of chitosan is essential for providing sufficient cationic polymers to encapsulate and reduce the metal ions.[29] Figure 3 shows the effect of acetic acid on the average particle size of Ag nanoparticles. As the concentration of acetic acid increases, the average particle size decreases, (Table 3). This observation aligns with our previous discussion: dissolving more chitosan means more sites are available for nanoparticle reduction. Chitosan, a

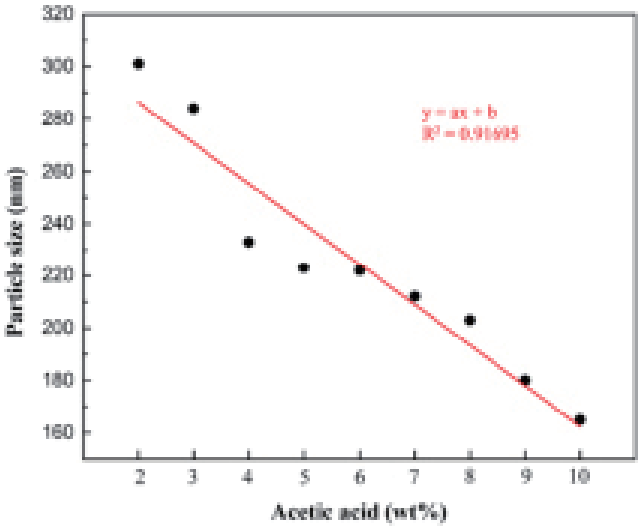

Fig. 3. (Color online) Effect of acetic acid concentration on average silver nanoparticle size .

Table 3
Experimental parameters of pH effect on silver particle size.

Sample	Ag PDF 00-004-0788, d-spacing (Å)	Calculated D (Å)	(h k l)
C2A2	301	3.93	210
C2A3	284	3.67	88
C2A4	233	3.40	64
C2A5	223	3.28	99
C2A6	222	3.14	66
C2A7	212	3.03	77
C2A8	203	2.90	56
C2A9	180	2.87	54
C2A10	165	2.80	60

biopolymer that is soluble in dilute acids owing to the protonation of its amine groups, acts as a stabilizing and reducing agent for silver ions in solution. Stabilizing refers to chitosan's capability to prevent the aggregation of silver nanoparticles by forming a protective layer around them using its amino and hydroxyl groups, which interact with the particle surface via electrostatic and hydrogen bonding.

At higher acetic acid concentrations, chitosan is better dissolved, and thus, more amine groups are available for interaction with silver ions. This higher availability of protonated amine groups may lead to a more efficient reduction of silver ions to silver nanoparticles, and it can stabilize the nanoparticles more effectively. When silver ions are reduced and immediately stabilized by a large number of available cationic sites on chitosan, they are less likely to aggregate, leading to the formation of smaller nanoparticles.

3.3 Effect of chitosan concentration on metal particle size

Following the dissolution mechanism of chitosan, the first experiment was conducted using 10 wt% acetic acid as the first fixed variable. The aim of the second experiment was to determine the amount of chitosan powder that could be dissolved in this solution. Although theoretically, adding more chitosan could increase the number of sites for metal particle reduction, an excess of chitosan could make the colloidal solution too viscous. This viscosity could lead to particle agglomeration during reduction, affecting the particle size and worsening their dispersibility, which are detrimental to the SERS effect.[30] Thus, in this experiment, we sought to find the optimal amount of chitosan to add with the given concentration of acetic acid, aiming for the best ratio for subsequently enhancing the SERS effect. The experiment was conducted with chitosan amounts of 0.5, 1, 2, 3, and 4 (wt%). It was observed that the average particle size was optimal at C2A10, supporting our proposed mechanism, as shown in Table 4.

SEM images showed that even after centrifuging the colloidal solution to isolate the precipitated silver nanoparticles, the particles were clearly coated with chitosan and visibly agglomerated. When too little chitosan was added, although there were no issues with excessive viscosity, SEM images revealed a significant unevenness in particle size. The dissolution mechanism can explain this result: dissolving chitosan creates sites for particle reduction, but with less dissolved chitosan, fewer sites are created. Excess metal ions without chitosan coverage are left to reduce independently, resulting in uneven sizes. Particles at sites were reduced to the desired size, while those without chitosan for stabilization grew into larger particles, an undesired outcome. The experiment revealed that 2 wt% chitosan is the optimal concentration to be added to the colloidal solution.

Table 4
Experimental parameters used to determine chitosan concentration effect on metal particle size.

Sample	Average particle size (nm)	Standard deviation
C0.5A10	235	86
C1A10	229	79
C2A10	165	60
C3A10	255	82
C4A10	259	80

3.4 Dispersion of metal particles on SERS substrates

Reducing one silver ion per site can minimize the size of the nanoparticles maximally, and the complete encapsulation by cationic polymers allows for the formation of a uniform metallic nanoparticle colloidal solution through electrostatic solid interactions between particles. Chitosan, being a cationic polymer, plays a critical role in particle dispersion by providing a positive charge that attracts the negatively charged silver ions during the reduction process. This interaction promotes uniform nucleation and inhibits aggregation, resulting in controlled nanoparticle size and narrow size distribution. Furthermore, the cationic nature of chitosan enhances the stabilization of the nanoparticles by forming a robust electrostatic barrier, which reduces the likelihood of agglomeration even at high silver ion concentrations. After adding various amounts of silver nitrate for reduction and the formation of films, high-magnification optical microscopy images were taken, as shown in Figs. 4–8. In Fig. 4, the silver ions are highly

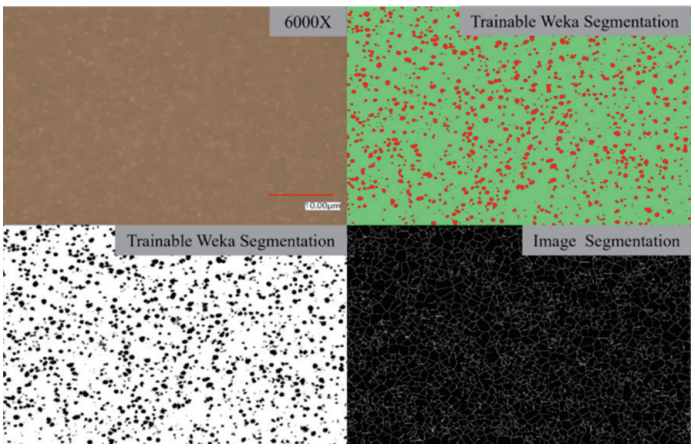

Fig. 4. (Color online) High-magnification image and postprocessed segmentation images of the C2S5 substrate.

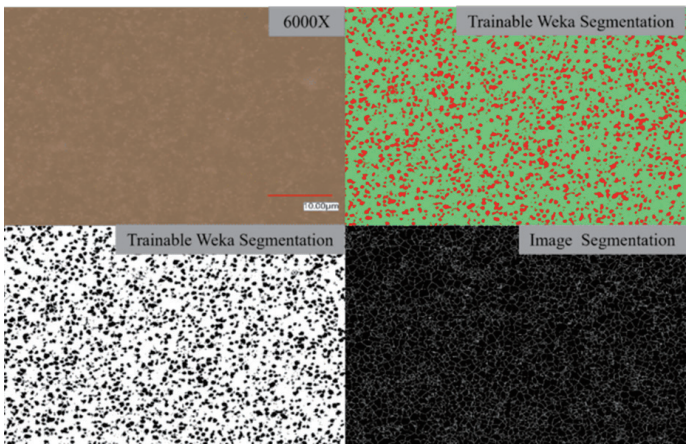

Fig. 5. (Color online) High-magnification image and postprocessed segmentation images of the C2S10 substrate.

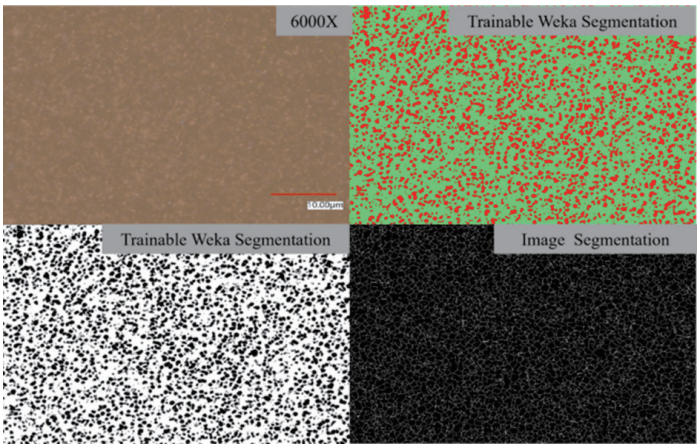

Fig. 6. (Color online) High-magnification image and postprocessed segmentation images of the C2S15 substrate.

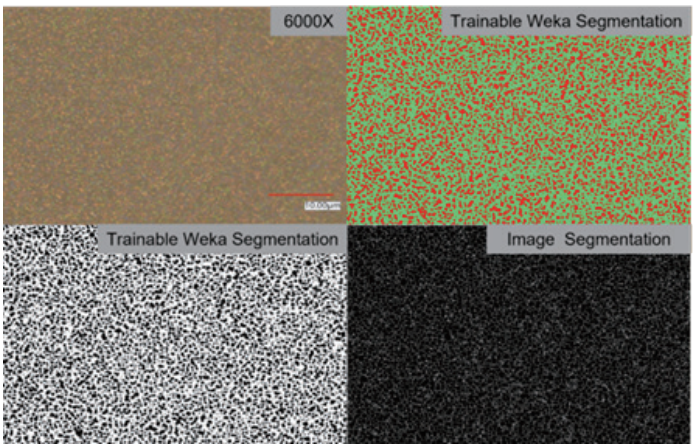

Fig. 7. (Color online) High-magnification image and postprocessed segmentation images of the C2S30 substrate.

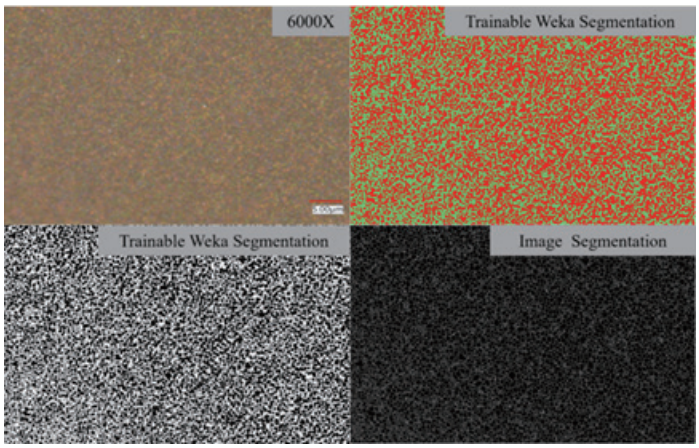

Fig. 8. (Color online) High-magnification image and postprocessed segmentation images of the C2S40 substrate.

dispersed owing to the creation of more sites than the amount of silver ions added, resulting in high dispersion. However, this level of distribution is still not sufficient for the goal of enhancing the signal strength on SERS substrates. Figure 8 shows that although the particles are densely packed, they maintain a certain distance from each other. This effectively demonstrates the successful creation of reduction sites and encapsulation by cationic polymers, allowing for evenly dispersed particles. This dispersion aligns with the objectives mentioned earlier regarding the creation of SERS substrates. Further experiments must be conducted to verify the relationship between the distribution and enhancement of Raman signal strength.

In these experiments, high-magnification optical microscopy was utilized for imaging, followed by postprocessing with ImageJ software to facilitate subsequent observation and calculation. Particle segmentation was performed using the software for measuring the segmented area XA, and the data were presented in a histogram format in which a normal distribution curve was established. The dispersion of particles, $D_{0.2}$, defined as the number of data points within a certain percentage of the mean value μ, was calculated. A higher D value indicates a more uniform dispersion, where the areas between particles are more evenly distributed. It was calculated using

$$D_k = \int_{\mu(1-k)}^{\mu(1+k)} f\left(x_A\right) da. \tag{1}$$

The distribution of silver nanoparticles under various parameters is shown in Figs. 5–9. As shown in Table 5, the dispersion of silver nitrate particles in C2S5 appears to be poor. This can

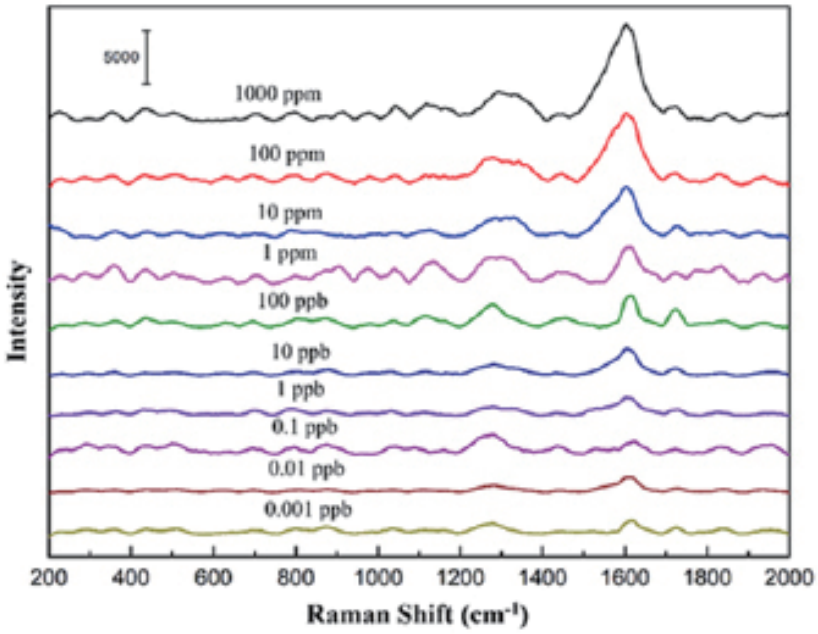

Fig. 9. (Color online) Detection limit test of SERS substrate.

Table 5
Experimental parameters used to determine the effect of silver nitrate on substrate dispersion.

Sample	Average particles area (nm^2)	$D_{0.2}$
C2S5	562.403	19.2
C2S10	293.921	21.8
C2S15	258.118	24.1
C2S30	193.165	30.2
C2S40	186.588	24.7

be explained by the mechanism previously discussed: a sufficient number of sites were created, but an insufficient number of silver ions were added, leading to the particles being highly dispersed, as shown in Fig. 5. With an increase in the number of silver ions added, the $D_{0.2}$ values improve, indicating better dispersion. This change in distribution can be intuitively perceived from the images.

Through the experiment, C2S30 was found to be the optimal amount for dispersion; the particles were densely packed yet maintained a certain distance from each other without agglomerating. This can be explained by the number of created sites being close to the number of added silver ions, achieving the ideal one site for one silver ion reduction and thus, optimal dispersion. However, at C2S40, despite the density of particles being higher, as shown in Fig. 9, the calculated $D_{0.2}$ value did not show improvement. This is because the added silver ions exceeded the number of sites, causing multiple particles to be reduced at a single location, leading to agglomeration. This is detrimental to the goal of enhancing dispersion.

3.5 SERS sensing performance using crystal violet dye

Initially, the crystal violet dye was used to determine the maximum detection limit of our fabricated SERS substrate. The dye is advantageous for analysis because of the simplicity of its preparation at various concentrations and its capability to yield strong Raman signals quickly. As shown in Fig. 9, our substrate detected signals at concentrations down to 0.1 ppb. However, below this concentration, there was no significant enhancement effect. Thus, it is inferred that the enhancement limit of this substrate reaches a maximum at 0.1 ppb. In subsequent detections, 0.1 ppb will be considered as the threshold limit for measurement.

Following this, substrates with varying degrees of dispersion were used to compare their SERS enhancement effects, employing the crystal violet dye's characteristic intensity at 1612 cm^{-1} to calculate the SERS enhancement factor (EF) using Eq. (2). The complete SERS performance is shown in Fig. 10. The relationship between SERS EF and $D_{0.2}$ is shown in Table 6. It is observed that there is a close correlation between $D_{0.2}$ and SERS EF; a higher $D_{0.2}$ indicates better substrate dispersion and, consequently, better SERS EF performance. The addition of a smaller amount of silver nitrate might result in a reduced average particle size but can lead to poor SERS enhancement effects due to the particles being too dispersed, as shown in Fig. 6. Conversely, as shown in Table 6, adding too much silver nitrate increases the average particle size and reduces $D_{0.2}$, leading to diminished SERS enhancement effects.

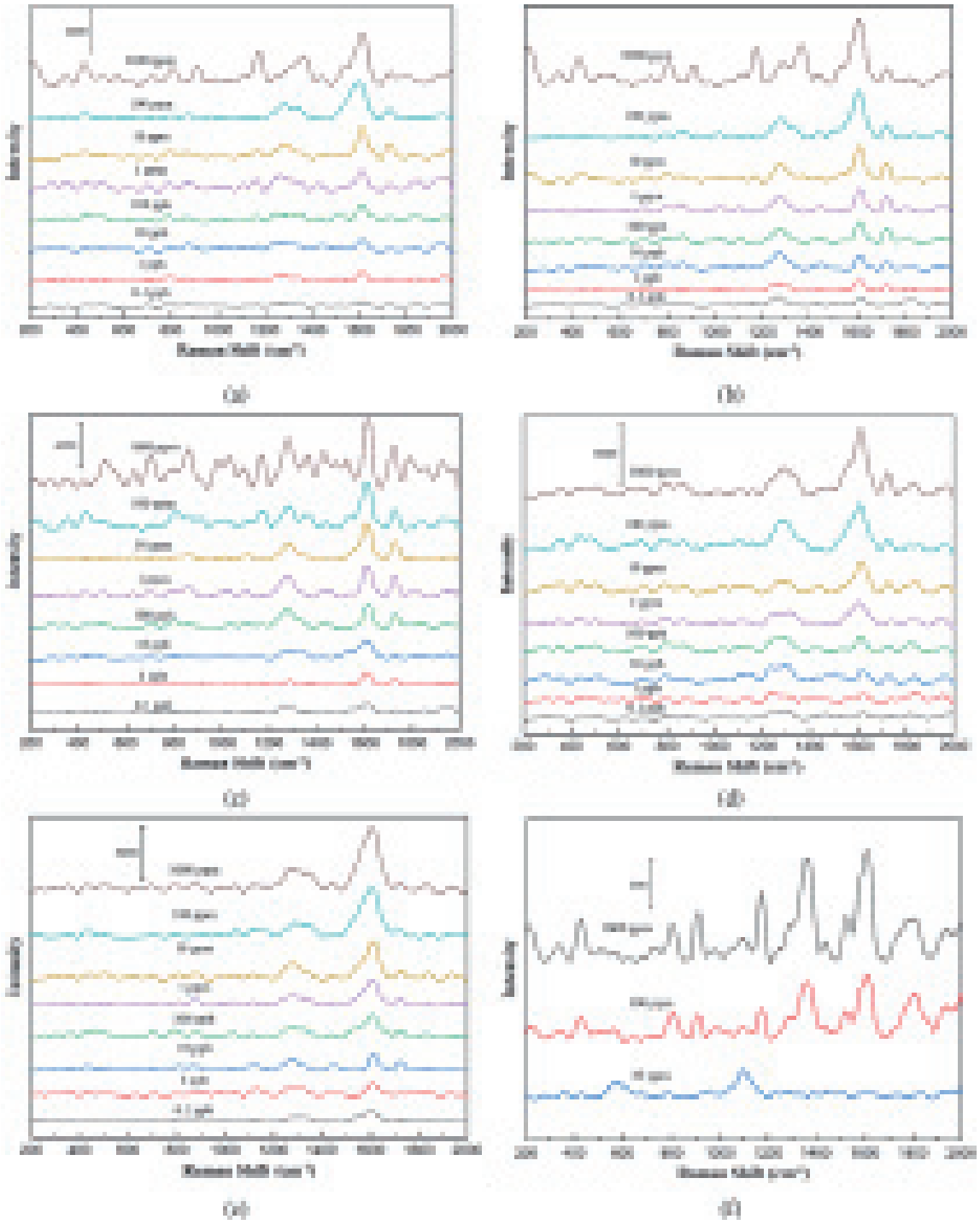

Fig. 10. (Color online) Detection of crystal violet dye on different substrates: (a) C2S5, (b) C2S10, (c) C2S15, (d) C2S30, (e) C2S40, (f) glass substrate.

Table 6
Experimental parameters used to determine dispersion effect on SERS EF.

Sample	Average particle size (nm)	$D_{0.2}$	SERS EF	Normalized
C2S5	158	19.2	3920093	1
C2S10	165	21.8	4273306	1.09
C2S15	171	24.1	4782860	1.22
C2S30	168	30.2	5893978	1.5
C2S40	191	24.7	5066589	1.29

$$EF = \frac{I_{SERS}}{N_{SERS}} \cdot \frac{N_{RS}}{I_{RS}} \tag{2}$$

The normalized data are all based on the SERS EF of C2S5 as the reference.

3.6 Detection of environmental hormone BPA

Figure 11 presents the Raman spectra, in which the characteristic Raman shift at 830 cm^{-1} corresponds to the detection of BPA. Table 7 shows the SERS EF values for each substrate. Among the five different SERS substrates tested, the highest enhancement effect was observed on the C2S30 substrate. After normalization, its EF enhancement effect was about 45% higher than the substrate with the lowest amount of silver nitrate. This clearly illustrates the significant impact of chitosan on the distribution of silver nitrate, and hence the performance of SERS substrates. The lowest detection limit for BPA powder was consistently found to be 0.1 ppb across all substrates. This result is ten times higher than those in a similar work.[31]

3.7 Detection of BPA in thermal paper

Figure 12 illustrates the detection of BPA in aqueous solutions using a SERS substrate integrated into thermal paper. The two most effective thermal paper samples in Table 7 were selected as the substrates for this analysis. A BPA concentration of 1 ppb was applied as the control. The presence of BPA was confirmed at a Raman shift of 830 cm^{-1} in both thermal paper samples. The chitosan–silver nitrate composite, employed as a SERS substrate, demonstrated significant enhancement effects. This was evidenced by the pronounced distinction in the Raman spectra of the thermal paper samples compared with the BPA control. These findings substantiate the notion that chitosan effectively stabilizes silver nanoparticles, thus amplifying the Raman signal intensity for BPA detection.

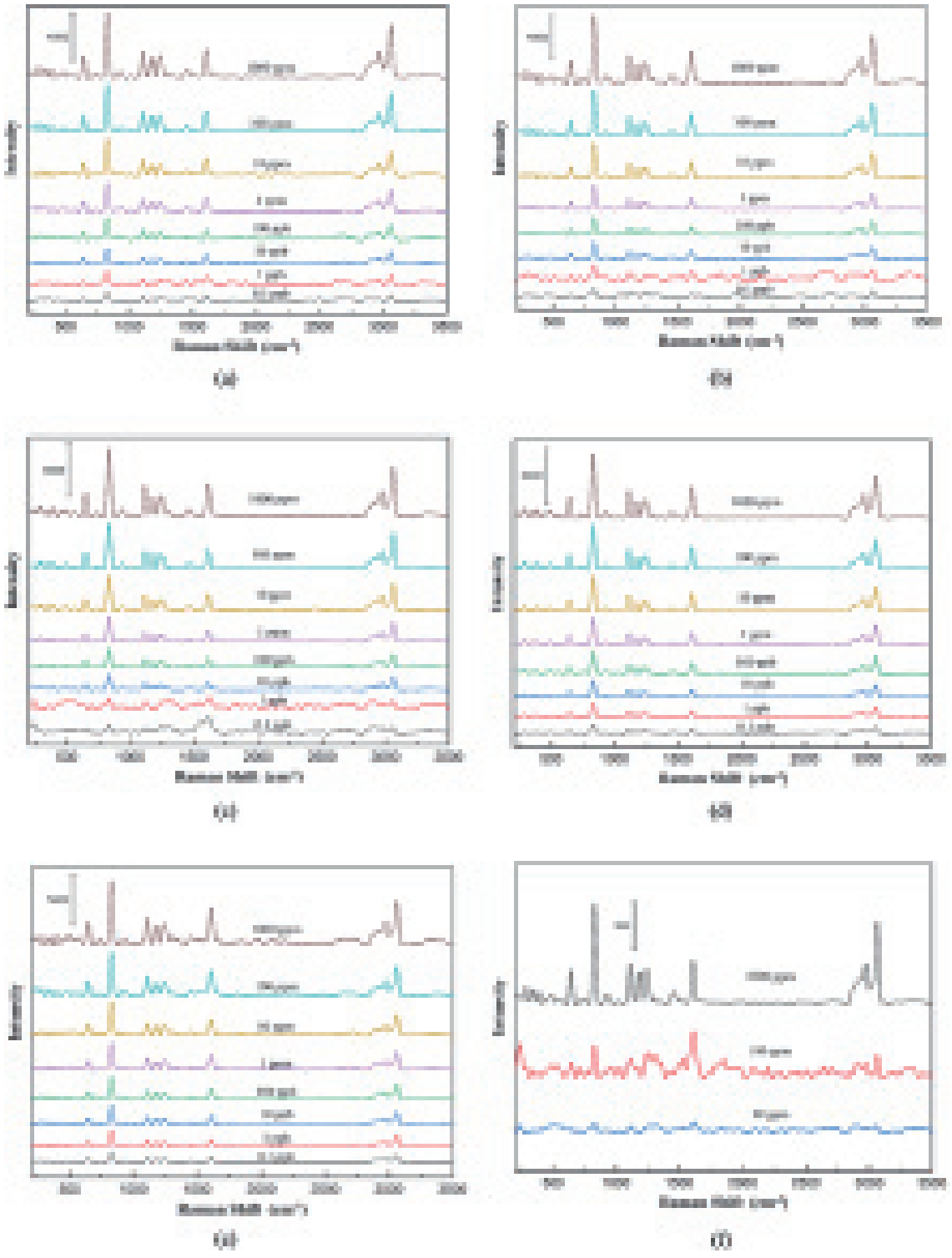

Fig. 11. (Color online) Detection of BPA on different substrates: (a) C2S5, (b) C2S10, (c) C2S15, (d) C2S30, (e) C2S40, (f) glass substrate.

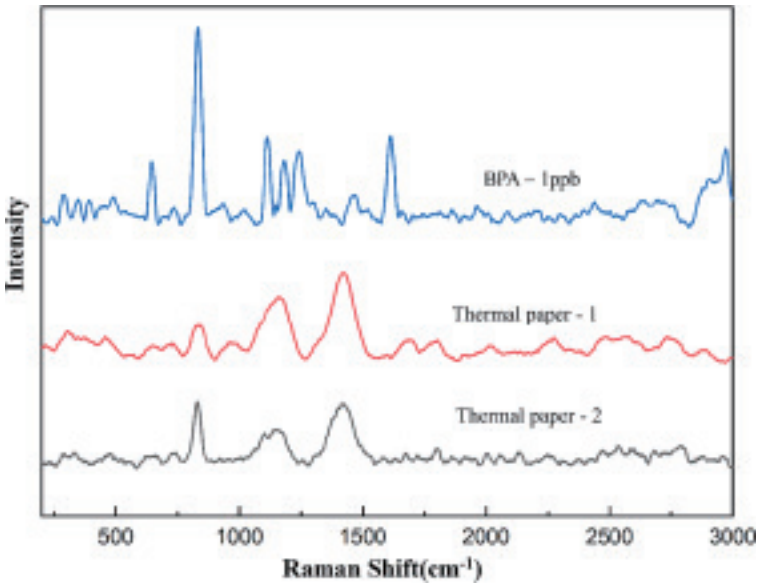

Fig. 12. (Color online) Raman spectra of BPA in aqueous solutions using a SERS substrate integrated into thermal paper.

Table 7
Experimental parameters used to determine the dispersion effect on SERS EF for BPA detection.

Sample	Average particle size (nm)	$D_{0.2}$	SERS EF	Normalized
C2S5	158	19.2	6313131	1
C2S10	165	21.8	7508418	1.18
C2S15	171	24.1	8164983	1.29
C2S30	168	30.2	9183502	1.45
C2S40	191	24.7	8572885	1.35

4. Conclusions

This research project was focused on creating a simple, one-step, environmentally friendly, green method for fabricating SERS substrates. The characteristics of chitosan as a cationic polymer were fully utilized by controlling the production parameters to create reduction sites for silver ions. The process involved enhancing the mechanical properties of the chitosan matrix by adding plasticizers to counteract chain scission, enabling the direct formation of films used as one-step SERS substrates for detection purposes. Chitosan was successfully used to reduce nanoparticles, and TEM images and diffraction patterns confirmed the FCC structure of silver nanoparticles. The acetylamino structure of chitosan was leveraged, and its solubility in the colloidal solution was enhanced by controlling the pH, thereby creating more sites for nanoparticle reduction and decreasing the particle size.

Higher chitosan concentrations in the colloidal solution provided more side-chain functional groups for comprehensive metallic core coverage, utilizing the strong electrostatic forces of the cationic polymer to inhibit particle agglomeration. However, concentrations above 2 wt% resulted in overly viscous solutions that hindered uniform reaction progress, while too low

concentrations failed to fully encapsulate metal cores, leading to aggregation and increased particle size. After creating reduction sites, adjusting the number of silver ions added for nanoparticle reduction was vital. Too little addition resulted in the failure to utilize all sites, causing excessive dispersion; too much caused aggregation at the same spot, worsening dispersion. The abundant OH groups of polyols were used to bridge chitosan's chain scission, enhancing mechanical properties while adhering to the goal of green reduction.

The resulting one-step SERS substrate demonstrated its effectiveness as a sensitive and efficient sensor for BPA detection, with a detection limit of 0.1 ppb. This capability highlights the sensor's potential for real-time environmental monitoring of pollutants, particularly endocrine-disrupting chemicals like BPA. By converting heavy-metal pollutants to valuable resources for creating SERS substrate, this method offers a green and sustainable approach that could also be adapted for detecting other hazardous substances.

While the currently used substrates can detect target signals, future efforts will refine the reduction process based on the described mechanisms to further reduce the particle size and enhance SERS EF. Testing a sensor in complex environmental samples, such as seawater or wastewater, may provide insights into its effectiveness for real-world applications, potentially extending to the detection of microplastics and other pollutants. Additionally, research related to long-term stability should also be conducted in the future. Further potential applications include optimizing the sensor for detecting heavy metals in river water contaminated by industrial effluents. Such applications require further adjustments to enhance sensitivity and selectivity in diverse matrices. Additionally, the sensor could be adapted to measure pollutants in urban environments, such as stormwater or roadside runoff, to track sources of pollution. In cold regions, optimizing the sensor for low-temperature conditions would ensure reliability in harsh environmental settings. This versatile sensor technology shows promise not only in environmental protection but also in advancing sustainable waste management through innovative nanotechnology applications.

Acknowledgments

This work was supported by the National Science and Technology Council, Taiwan (grants number 112-2221-E-006-173, 113-2221-E-006-087-MY2, 113-2221-E-006-112-MY2, and 113-2221-E-006-116). The authors gratefully acknowledge the Core Facility Center of National Cheng Kung University for allowing us to use their EM000700 equipment. This research was partly supported by the Higher Education Sprout Project, Ministry of Education to the Headquarters of University Advancement at National Cheng Kung University (NCKU).

References

1 H. Mohajan: J. Social Sci. Humanit. **5** (2019) 377.
2 J. A. Brandon, W. Jones, and M. D. Ohman: Sci. Adv. **5** (2019) eaax0587. https://doi.org/10.1126/sciadv.aax0587
3 L. López-Carrillo, Á. Mérida-Ortega, H. Gómez-Ruiz, L. Hernández-Garciadiego, and B. Gamboa-Loira: Int. Arch. Occup. Environ. Health **94** (2021) 699. https://doi.org/10.1007/s00420-020-01590-x
4 M. Alsen, C. Sinclair, P. Cooke, K. Ziadkhanpour, E. Genden, and M. van Gerwen: Toxics **9** (2021) 14. https://doi.org/10.3390/toxics9010014

5 R. Naomi, M. D. Yazid, H. Bahari, Y. Y. Keong, R. Rajandram, H. Embong, S. H. Teoh, S. Halim, and F. Othman: Int. J. Mol. Sci. **23** (2022) 2969. https://doi.org/10.3390/ijms23062969
6 X. Wang, Y. Wu, X. Wen, X. Bai, Y. Qi, L. Zhang, H. Yang, and Z. Yi: Opt. Mater. **121** (2021) 111536. https://doi.org/10.1016/j.optmat.2021.111536
7 L. Xiao, S. Feng, M. Z. Hua, and X. Lu: Talanta **254** (2023) 124128. https://doi.org/10.1016/j.talanta.2022.124128
8 S.-C. Shi, S.-W. Ouyang, and D. Rahmadiawan: Polymers **16** (2024) 960. https://doi.org/10.3390/polym16070960
9 X. Liu, J. Guo, Y. Li, B. Wang, S. Yang, W. Chen, X. Wu, J. Guo, and X. Ma: J. Mater. Chem. B **9** (2021) 8378. https://doi.org/10.1039/D1TB01299A
10 J. Li, Y. Feng, L. Liang, F. Liao, W. Huang, K. Li, G. Cui, and Z. Zuo: ACS Appl. Mater. Interfaces **16** (2024) 35771. https://doi.org/10.1021/acsami.4c05642
11 H. Nurdin, W. Waskito, A. N. Fauza, B. M. Siregar, and B. K. Kenzhaliyev: Teknomekanik **6** (2023) 94. https://doi.org/10.24036/teknomekanik.v6i2.25972
12 D. Rahmadiawan, Z. Fuadi, R. Kurniawan, H. Abral, F. Ilhamsyah, A. Arafat, R. Rifelino, B. Syahri, and E. Indrawan: Tribol. Ind. **44** (2022) 584. https://doi.org/10.24874/ti.1357.08.22.10
13 D. Rahmadiawan and S.-C. Shi: Sci. Rep. **14** (2024) 9217. https://doi.org/10.1038/s41598-024-59010-w
14 D. Rahmadiawan, S. C. Shi, Z. Fuadi, H. Abral, N. Putra, R. Irwansyah, D. Gasni, and A. M. Fathoni: J. Tribologi **39** (2023) 36.
15 S.-C. Shi, F.-I. Lu, C.-Y. Wang, Y.-T. Chen, K.-W. Tee, R.-C. Lin, H.-L. Tsai, and D. Rahmadiawan: Int. J. Biol. Macromol. **264** (2024) 130547. https://doi.org/10.1016/j.ijbiomac.2024.130547
16 A. Jiang, R. Patel, B. Padhan, S. Palimkar, P. Galgali, A. Adhikari, I. Varga, and M. Patel: Polymers **15** (2023) 2235. https://doi.org/10.3390/polym15102235
17 Y. Zaiki, A. Iskandar, and T. W. Wong: Biotechnol. Adv. **67** (2023) 108200. https://doi.org/10.1016/j.biotechadv.2023.108200
18 I. Aranaz, A. R. Alcántara, M. C. Civera, C. Arias, B. Elorza, A. Heras Caballero, and N. Acosta: Polymers **13** (2021) 3256. https://doi.org/10.3390/polym13193256
19 C. Puente, M. Sánchez-Domínguez, C. L. Brosseau, and I. López: Mater. Chem. Phys. **260** (2021) 124107. https://doi.org/10.1016/j.matchemphys.2020.124107
20 S.-C. Shi and J.-Y. Wu: Surf. Coat. Technol. **350** (2018) 1045. https://doi.org/10.1016/j.surfcoat.2018.02.067
21 S.-C. Shi, C.-F. Chen, G.-M. Hsu, J.-S. Hwang, S. Chattopadhyay, Z.-H. Lan, K.-H. Chen, and L.-C. Chen: Appl. Phys. Lett. **87** (2005) 203103. https://doi.org/10.1063/1.2128484
22 S.-C. Shi, T.-H. Chen, and P. K. Mandal: Polymers **12** (2020) 1246. https://doi.org/10.3390/polym12061246
23 X. Wang, W. Ning, K. Wang, and D. Yu: Sustainability **15** (2023) 165. https://doi.org/10.3390/su15010165
24 I. Hamada, T. Kumagai, A. Shiotari, H. Okuyama, S. Hatta, and T. Aruga: Phys. Rev. B **86** (2012) 075432. https://doi.org/10.1103/PhysRevB.86.075432
25 C. K. Reddy, E. S. Jung, S. Y. Son, and C. H. Lee: LWT **131** (2020) 109723. https://doi.org/10.1016/j.lwt.2020.109723
26 A. Hamed, D. Ghareeb, T. M. Mohamed, M. Hamed, M. S. Nofal, and M. Gaber: BMC Complementary Med. Ther. **23** (2023) 384. https://doi.org/10.1186/s12906-023-04212-4
27 R. Konakanchi, P. Jyothi, and L. R. Kotha: Polycyclic Aromat. Compd. **42** (2021) 226. https://doi.org/10.1080/10406638.2020.1725899
28 F. Hua, T. Yao, and Y. Yao: Sensors **24** (2024) 1789. https://doi.org/10.3390/s24061789
29 U. Upadhyay, I. Sreedhar, S. A. Singh, C. M. Patel, and K. L. Anitha: Carbohydr. Polym. **251** (2021) 117000. https://doi.org/10.1016/j.carbpol.2020.117000
30 X. Li, W. Chen, and C. Zou: Powder Technol. **361** (2020) 957. https://doi.org/10.1016/j.powtec.2019.10.106
31 S. Chang, S. L. Eichmann, T.-Y. S. Huang, W. Yun, and W. Wang: J. Phys. Chem. C **121** (2017) 8070. https://doi.org/10.1021/acs.jpcc.7b00688